Performances of C-BORD's tagged neutron inspection system for explosives and illicit drugs detection in cargo containers

A. Sardet, B. Perot, C. Carasco, Guillaume Sannié, S. Moretto, G. Nebbia, C. Fontana, F. Pino

Performances of C-BORD's Tagged Neutron Inspection System for Explosives and Illicit Drugs Detection in Cargo Containers

A. Sardet, B. Pérot, C. Carasco, G. Sannié, S. Moretto, G. Nebbia, C. Fontana, F. Pino

***Abstract*– In the frame of the C-BORD project (H2020 program of the EU), a Rapidly Relocatable Tagged Neutron Inspection System (RRTNIS) has been developed for a nonintrusive inspection of cargo containers, aimed at explosives and other illicit goods detection. Twenty large volume NaI detectors are used to determine the elements composing inspected materials from their specific gamma spectra signatures induced by fast neutrons. The RRTNIS inspection is focused on a specific suspect area selected by X-ray radiography. An unfolding algorithm decomposes the energy spectrum of this suspect area on a database of pure element gamma signatures. A classification is then performed between inorganic materials, such as metals, ceramics or chemicals, and organic materials like wood, fabrics or plastic goods. Concerning organic materials, the obtained elemental proportions of carbon, nitrogen, and oxygen allow discriminating explosives from illicit drugs and benign substances. This paper reports on the final laboratory tests performed at CEA Saclay, France, to assess the RRTNIS detection performances before further demonstration tests in a real seaport environment. Simulants of explosives and illicit drugs have been hidden at different depths inside iron or wood cargo materials, which are representatives of the different neutron and gamma attenuation properties encountered in real cargo containers. Hundreds of experiments have been performed, showing that a few kg of explosives or narcotics can be detected by the RRTNIS in 10 min inspections.**

***Index Terms*— Associated Particle Technique, cargo containers, fast neutron inspection, homeland security.**

I. Introduction

THE C-BORD European project [1], [2] of H2020 Research and Innovation Program aimed at developing a system of non-intrusive inspection technologies for cargo containers, to fight against illicit trafficking like CBRNE (Chemical, Bacteriological, Radiological, Nuclear, Explosive) threats, cigarettes, narcotics, and any other contraband materials. C-BORD combines five complementary technologies to offer a wide range of detection capabilities: radiation portal monitors, X-ray scanners, tagged neutron inspection, photofission, and trace gas analyzers.

This paper reports on the final laboratory tests performed at CEA Saclay to estimate the performances of the Rapidly Relocatable Tagged Neutron Inspection System (RRTNIS) before the demonstration field tests, in a real seaport environment. In the C-BORD framework, the RRTNIS is used as second line inspection system, when a suspect area was first localized with the primary X-ray scanner. For instance, it helps distinguishing organic substances (explosives vs. narcotics vs. benign materials) with similar densities and atomic numbers, which look similar on the X-ray radiography.

The RRTNIS is based on the Associated Particle Technique [3] (APT), which allows the identification of the elements constituting the inspected cargo materials from gamma rays induced by fast neutron, as detailed in the next section. Compared to the previous EURITRACK system [4], which was a fixed portal with thick concrete walls to ensure radiological shielding in the environment of the seaport of Rijeka, the RRTNIS is compact and transportable, as described in [5] and in section II. Thanks to a thick polyethylene block around the DT neutron generator (14 MeV neutrons), the restricted area, at the border of which the dose rate is about 1 $\mu Sv.h^{-1}$ (for non-radiation workers), extends to 40 m × 60 m without a beam dump, or 40 m × 40 m with a polyethylene wall in front of the beam. This allows a quick implementation of the RRTNIS in any seaport or border control point, where an area of this size is available. Compared to a large neutron inspection system like PFNA [6], which allows a full 3D elemental characterization of cargo materials by a complete scanning of the container, the RRTNIS focusses neutron inspection with the APT on a suspicious area determined by the X-ray scanner. This greatly limits investment and operational costs of the system, but also activation of cargo containers and the dose deposited in transported goods.

II. Development of the C-BORD RRTNIS

A neutron generator, operated at 10^8 $n.s^{-1}$, is used to produce 14 MeV neutrons with the $d + {}^3H \rightarrow n + \alpha$ fusion reaction. As the alpha particle is emitted almost back-to-back with the neutron, the use of a position sensitive YAP scintillator enables a spatial selection of interrogating fast neutrons, as shown in Fig. 1.

Manuscript received November 28, 2019. This work has received funding from the European Union's Horizon 2020 research and innovation program under grant agreement No 653323. This text reflects only the author's views and the Commission is not liable for any use that may be made of the information contained therein.

A. Sardet, B. Pérot and C. Carasco are with CEA, DEN, Cadarache, DTN, SMTA, Nuclear Measurement Laboratory, F-13108 Saint-Paul-lez-Durance, France (email: alix.sardet@cea.fr).

G. Sannié is with CEA, DRT, LIST, Saclay, F-91191 Gif-Sur-Yvette, France.

S. Moretto, G. Nebbia, C. Fontana and F. Pino are with Dipartimento di Fisica e Astronomia, INFN di Padova, via Marzolo, 8, I-35131 Padova, Italy.

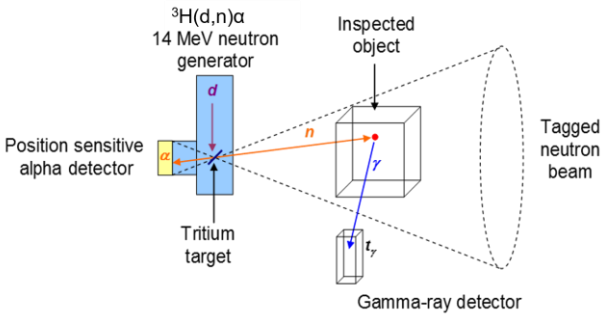

Fig. 1. Principle of the Associated Particle Technique.

The neutron generator is encased in a polyethylene shield to ensure radiation protection, as illustrated in Fig. 2, which represents the RRTNIS designed in the C-BORD project [5]. The tagged neutron cone, with a total aperture angle of 20°, escapes from the polyethylene shield through a conical hole. Gamma rays resulting from tagged neutron interactions within the inspected material are detected by twenty 5"×5"×10" parallelepiped-shaped NaI and four 3"×3" cylindrical $LaBr_3$ detectors (which will not be discussed in this paper) [7], [8] placed in a backscatter position, i.e. near the neutron generator. In addition, the coincidence time between the alpha and the neutron-induced gamma detections allows determining the neutron time of flight, and subsequently its distance to interaction by assuming that all interactions occur along the beam axis and a constant neutron velocity of 5.13 $cm.s^{-1}$ (14 MeV neutrons). In practice, neutrons lose energy by elastic scattering, especially in rich-in-hydrogen cargo materials, which reduces their velocity. This cause a peak broadening in the flight path spectra (see further Fig. 7, panels c and d) but the associated bias is quite limited. Indeed, if energy loss is too high, interrogating neutrons cannot produce gamma rays by inelastic scattering and other fast-neutron reactions. By combining information on the direction of the neutron and its travelled distance, the gamma spectrum of any elementary volume (voxel) in the container can be reconstructed. In this way, it is possible to focus neutron inspection on any suspicious region determined on the X-ray radiography, in view to limit both measurement time and dose delivered to cargo containers, compared to full truck inspection systems [6].

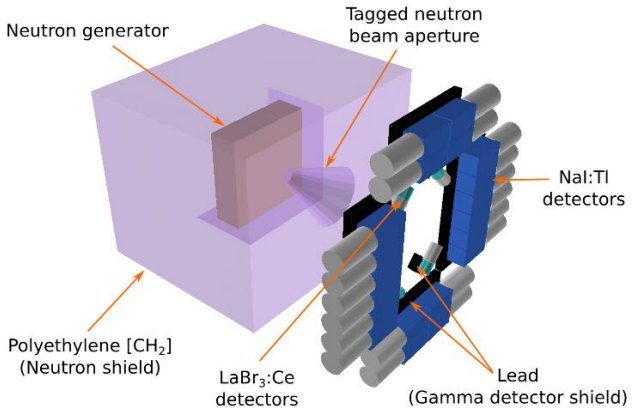

Fig. 2. Schematic view of C-BORD RRTNIS design [2].

Finally, the gamma spectrum of the voxel of interest is unfolded into a linear combination of elementary gamma spectra. These elementary gamma spectra are neutron-induced signatures measured during the RRTNIS calibration phase with pure element targets, as for instance graphite for carbon signature, liquid nitrogen, and water for oxygen (as fast neutrons do not produce gamma ray on hydrogen). Iron, lead, copper, aluminium, zinc, and other pure metals were also used, as well as some compounds when materials with pure elements were not (easily) available, such as NaCl for chlorine (after subtraction of Na signature measured with pure sodium), C_2F_4 for fluorine (after subtraction of carbon spectrum), H_3PO_4 for phosphorus and KOH for potassium (oxygen subtraction), etc. Fig. 3 shows the setup of pure element acquisitions performed at CEA Cadarache, France [9], with a limited number of detectors originating from previous EURITRACK [10] and UNCOSS [11] projects, and with a legacy TPA17 neutron generator (SODERN) from a former CEA project [12]. For each NaI or $LaBr_3$ detector, a correlation between the neutron TOF and the deposited gamma energy is computed. Using this correlation, a TOF (or neutron flight path) selection on the target is performed, to obtain the experimental gamma signature of the interrogated material. Fig. 4 presents the recorded gamma signatures for carbon, nitrogen and oxygen on NaI detectors. For more details, the reader is referred to [9].

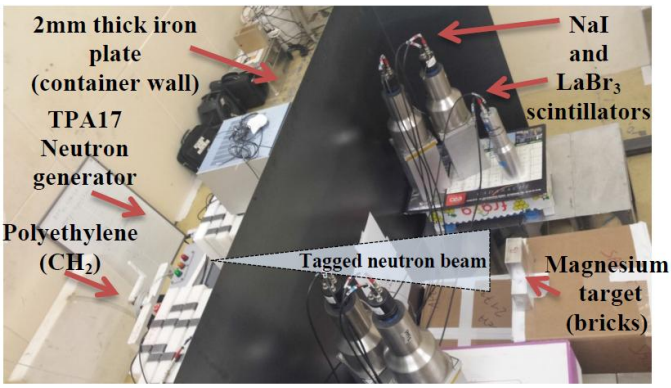

Fig. 3. Experimental setup to acquire pure element gamma signatures at CEA Cadarache. A 5 cm thick lead screen (not visible in the picture, between polyethylene and the iron wall) is used to shield gamma detectors.

After these first laboratory tests, the whole C-BORD detectors and data acquisition electronics [7], [8], as well as the polyethylene shield (visible with the conical aperture for tagged neutrons) and the lead shield, have been integrated and tested at JRC Ispra, Italy, see Fig. 5.

Finally, these core components of the RRTNIS have been integrated in a waterproof container (in view of future field tests in seaports) at CEA Saclay, France, see Fig. 6. The RRTNIS has been thoroughly tested with a wide range of test objects, for instance by concealing simulants of explosives, illicit drugs, and chemical elements used in chemical warfare, inside wood and iron matrixes, mimicking organic and metallic cargo materials. In this paper, we report only on results obtained with the twenty NaI detectors, as data from $LaBr_3$ detectors has not been processed yet. It will be in future

work, in view to detect specific chemical warfare signatures that are not present in NaI spectra, such as arsenic and bromine [13].

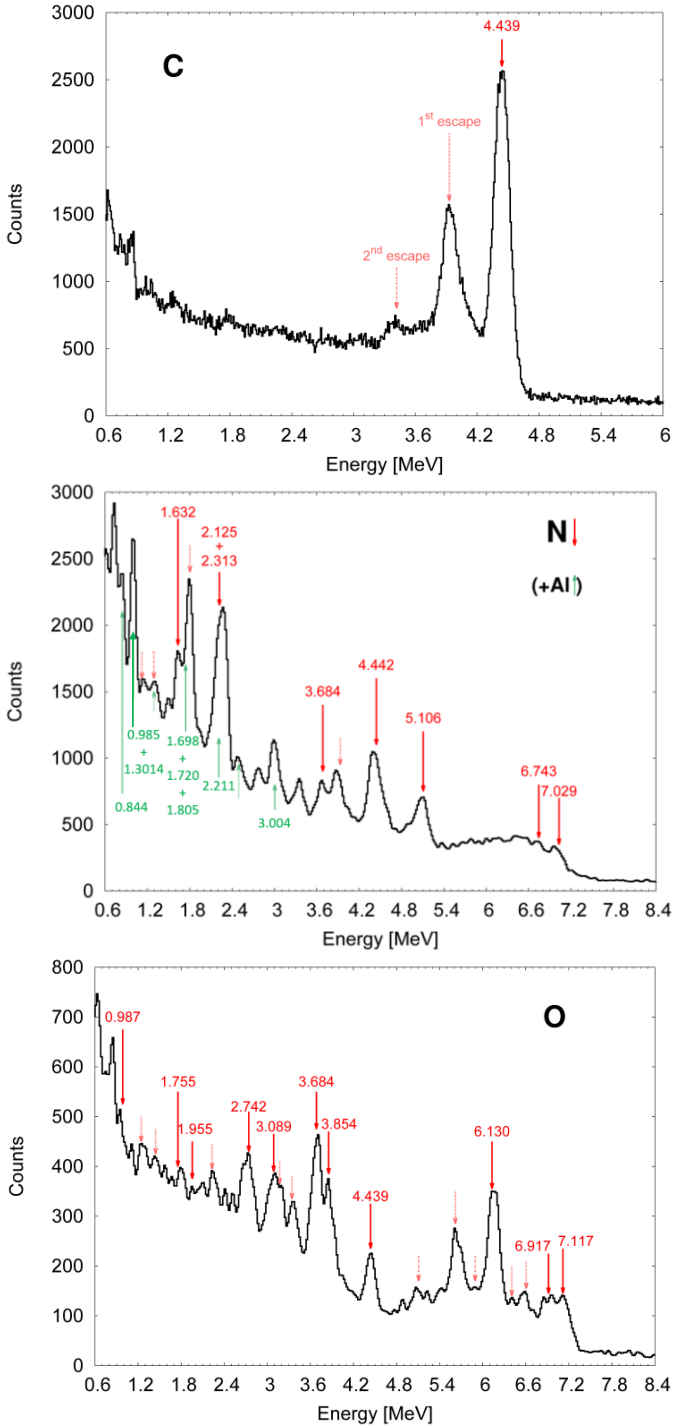

Fig. 4. Experimental gamma signatures of carbon (top), nitrogen (middle) and oxygen (bottom) on NaI detectors. Dashed arrows are used to point at peaks corresponding to first escapes, while dotted arrows are used for second escapes. On the nitrogen spectrum, the aluminum signature due to the cryogenic storage Dewar has not been subtracted yet (green up-arrows) [9].

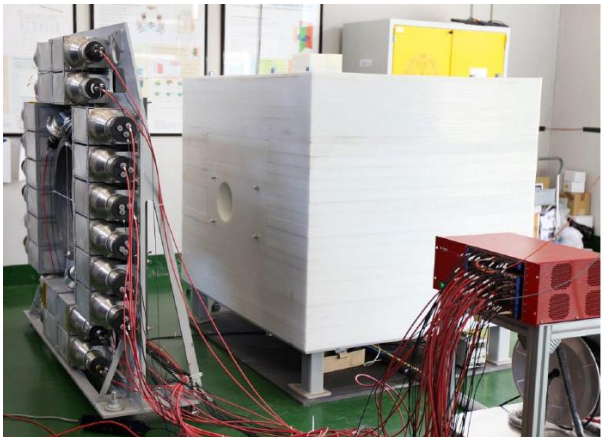

Fig. 5. Integration of the main components of C-BORD's RRTNIS at JRC Ispra, Italy.

Fig. 6. Integration of C-BORD RRTNIS components in a temperature-controlled and sealed container (in view of further outdoor field tests) at CEA Saclay, France.

III. Data Processing

To illustrate the complete data processing with the RRTNIS, this section fully describes the analysis of an inspection example with a C4 target (9 kg) hidden in a 0.2 g.cm^{-3} iron matrix, at a depth of 26 cm from the container wall. As explained in the previous section, the general objective of data processing is to select an appropriate tagged neutron beam (electronics collimation with the position sensitive alpha detector) to focus on a suspicious area defined on the X-ray radiography. After applying this selection, the neutron-induced gamma spectra at different depths inside the container is built using the TOF information converted into neutron flight path. Finally, a spectroscopic analysis is performed in view to classify and identify inspected materials.

Data received from the "ABCD" acquisition software [7] is treated on-line to reconstruct both the alpha distribution on the position sensitive YAP detector (see Fig. 1 and Fig. 7 (a)), which is used to perform the tagged neutron selection, and compute the neutron flight path vs. gamma energy 2D map (see Fig. 7 (b)).

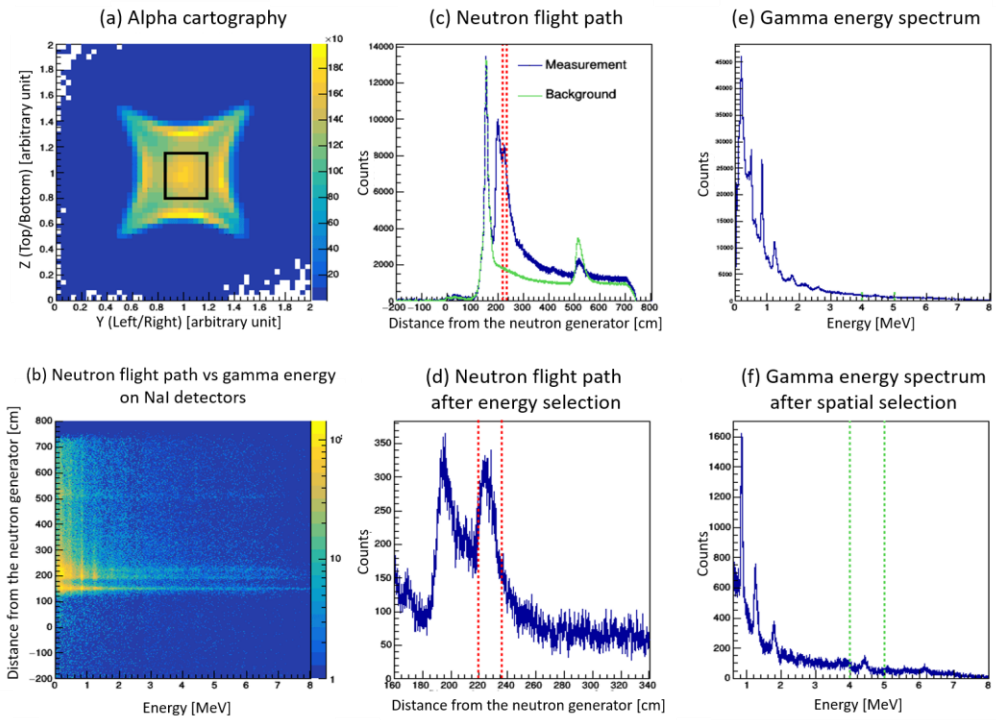

Fig. 7. Panel (a) represents the alpha cartography (coordinates on the ∅ 5 cm position sensitive YAP detector) with the alpha selection for this measurement (black rectangle). Panel (b) is the neutron flight path vs. gamma energy 2D map for the NaI detectors. The middle and right panels represent respectively projections on the neutron flight path axis ((c) and (d)) and on the energy axis ((e) and (f)) without ((c) and (e)) and with a selection ((d) and (f)) on the gamma energy (resp. the neutron position), after correction of the random background and of the correlated background (only for panel (f)). The spatial and energy selections are represented respectively by the red dashed lines and by the green ones. The green distribution on the total neutron flight path (panel (c)) corresponds to the flight path distribution of the correlated background.

Measurements performed at JRC Ispra evidenced that the background has two components: a random component, which can be estimated by the average number of counts at a given energy for negative (i.e. non-physical) distances; and a correlated component, caused by tagged neutron interactions on the surrounding materials. To correct for the latter, a measurement is performed without a container nor a target in front of the tagged neutron beam. The corresponding neutron flight path is shown in green on Fig. 7 (c) and in red on Fig. 8. As the neutron flight path does not depend on the measured object (cargo container or calibration target) between -100 cm and +180 cm (i.e. the end of the external case), the integral of counts in this area is computed on both the measurements with and without target for normalization purposes. The ratio of these integrals is then used to scale the background 2D map, before subtracting it to that of the cargo container (or any calibration target) measurement. Beyond 500 cm from the neutron generator is the wall of the irradiation cell. When a container is placed in front of the tagged neutron beam, it effectively slows down, and even stops, neutrons. Thus, the neutron beam is attenuated and the measured signal from the wall of the irradiation cell becomes smaller than that measured without any obstacle on the beam path.

After the background correction, an automatic procedure slices the neutron flight path in 10 cm width sections, with a 5 cm step. The resulting gamma spectrum is then unfolded using a least-square algorithm that decomposes the spectra into a linear combination of the pure elements gamma signatures. The retrieved weights give information on the composition of the target.

In view to further assess the uncertainties related to counting statistics, one hundred "synthetic" spectra are generated for the gamma spectrum of each slice. To this end, each channel of the gamma spectrum is sampled according to a Poisson distribution, with a mean equal to the number of counts in said channel.

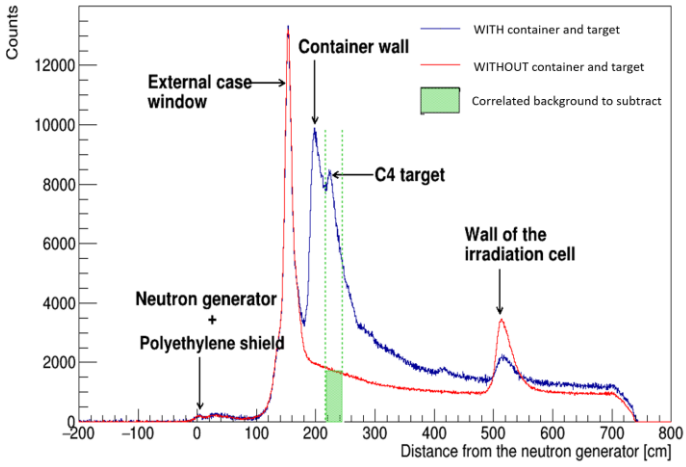

Fig. 8. Comparison of the neutron flight path for the measurement of a 9 kg C4 target dissimulated at 26 cm in depth in an iron filled container (in blue) and the neutron flight path for a measurement without a container or a target (in red). The presence of a correlated neutron background is observed.

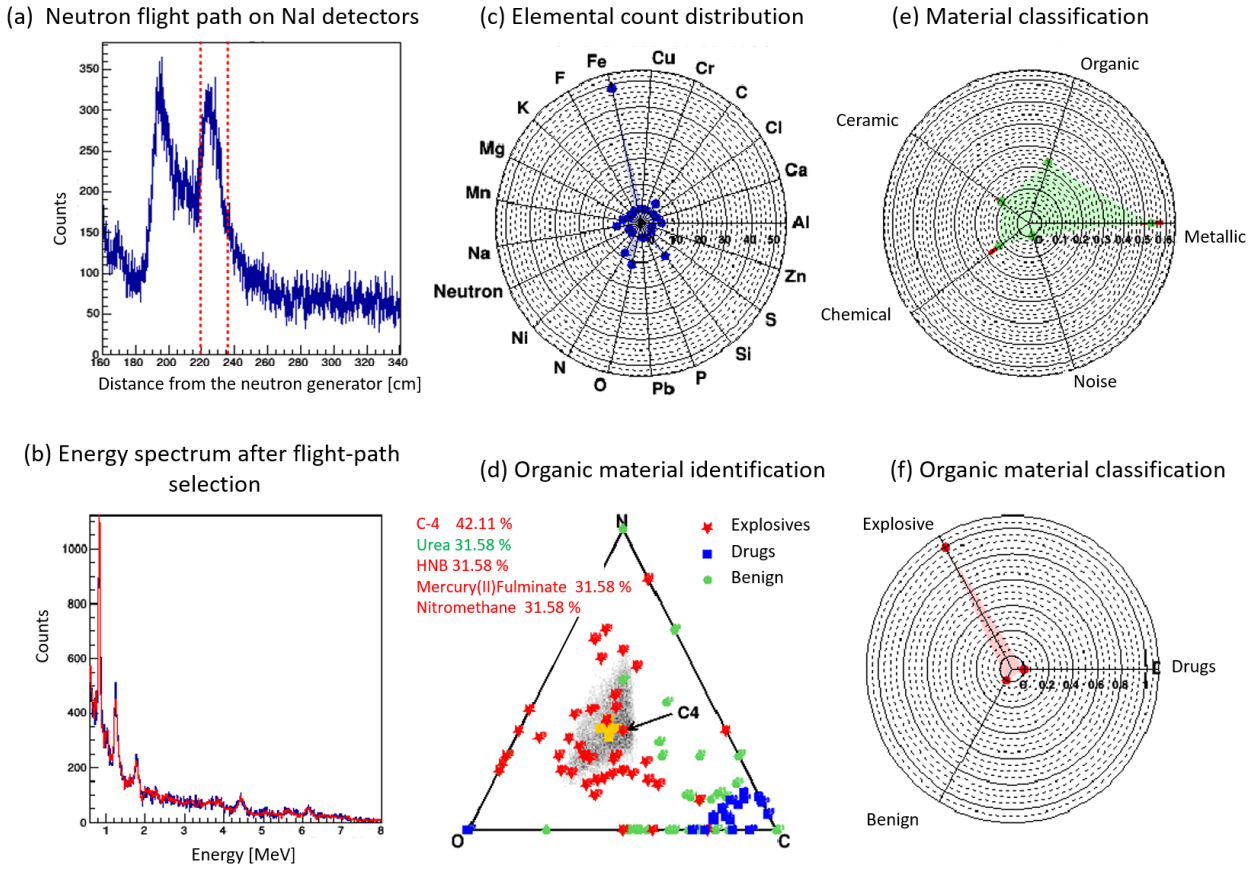

Fig. 9. Data analysis dashboard with panel (a) the neutron flight path spectrum after background subtraction (see Fig. 8); panel (b) the gamma spectrum of inspected materials located at a distance between 220 cm and 230 cm from the neutron generator (flight-path selection of panel (a), between the red dashed lines), and the result of the unfolding procedure (red line) obtained with the least square algorithm; panel (c) the elemental count proportions resulting from the unfolding; panel (d) the classification of organic materials according to their relative C, N and O proportions, in which the area in grey-scale corresponds to the measurement result with its uncertainties on the C, N and O proportions, see text for details; panel (e) another classification between the main cargo material categories, based on the elemental count proportions of panel (c) and in which "noise" corresponds to the proportion of the spectrum associated to the background, see the text for details; and panel (f) an alternative representation of the measurement result of panel (d) based on the 2D uncertainty area, see text for details.

The unfolding procedure is repeated for each of these hundred spectra, thus building a count fraction distribution for each of the pure elements present in the database (see Fig. 9 (c)).

In order to perform a coarse material classification, each pure element of the database is associated with a material type: chemical (calcium, chlorine, fluorine, etc.), ceramic (silicon), metallic (aluminium, iron, chromium, etc.) or organic (carbon, nitrogen and oxygen). The probability that the inspected target belongs to a given category is computed by calculating the ratio of the weights of the pure elements belonging to said category over the total sum of weights (see Fig. 9 (e)).

For organic materials, it is important to further refine the identification by differentiating between illicit drugs, explosives, and benign materials (such as wood or cotton). To do so, the unfolded weights for carbon, nitrogen and oxygen are transformed into chemical ratios [14], [15] using conversion factors. These conversion factors are determined by simulating the inspections of a 20 × 50 × 50 cm^3 TNT target (1.65 $g.cm^{-3}$, 80 kg) located in nine different positions (see Fig. 10) of a container filled with several representative materials (iron, cotton, ceramic, etc.), with the MCNP6 code.

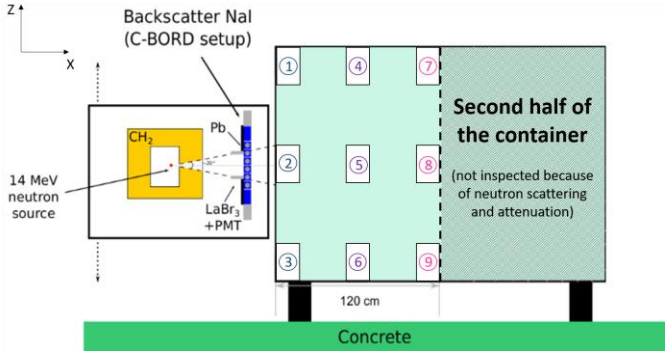

Fig. 10. Position of the TNT target used during the simulation of several inspection scenarios, to determine the conversion factors.

Using the PIKMT card of MCNP, gamma rays emitted by the carbon, nitrogen and oxygen atoms of the target were singled out from those produced on the same elements in organic cargo materials [15]. The resulting energy spectrum was unfolded and the ratio of the obtained count fractions to the real carbon, nitrogen, oxygen chemical proportions of

TNT gave the conversion factors to be used. However, as the energy of the

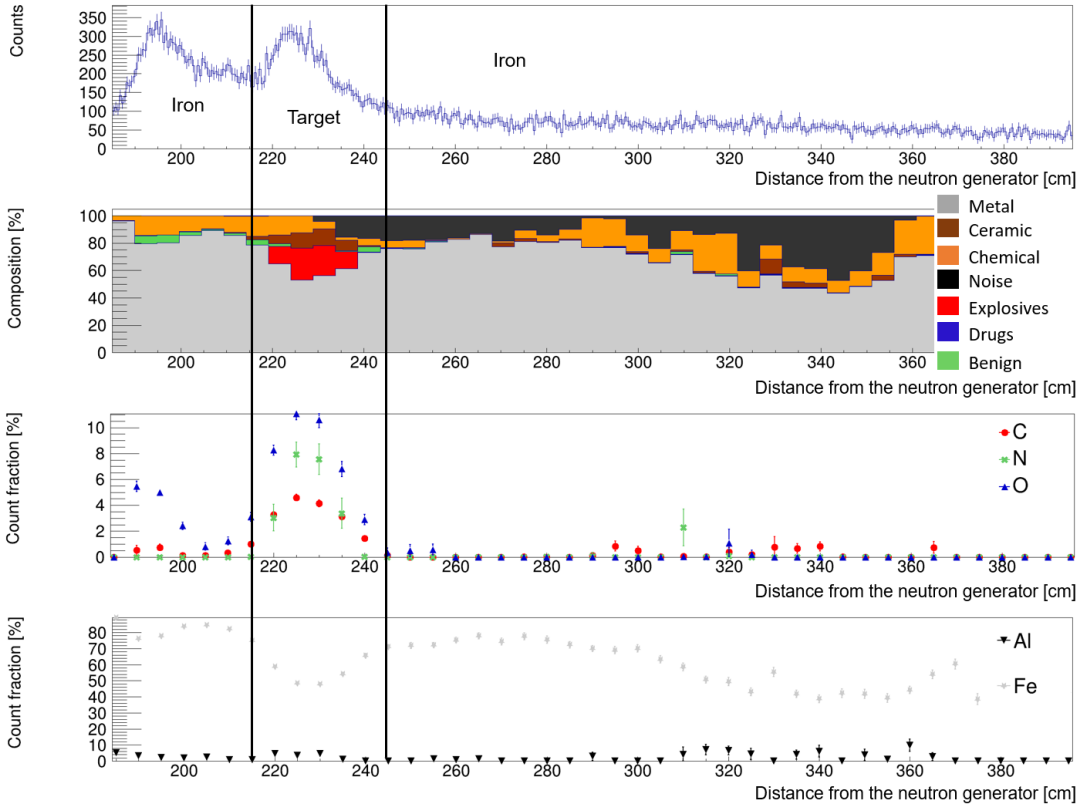

Fig. 11. Material and count fraction profiles obtained during the 10 min measurement of a 9 kg C4 target hidden behind 26 cm of iron matrix material. The red spot signs the presence of an explosive. It is correlated with an increase in carbon, nitrogen and oxygen count fractions, which are used to identify the C4 explosive (see triangle diagram of Fig. 9 (d)).

incident neutron beam changes with the increasing depth of the target in the container, due to neutron slowing down, so does the gamma signatures of the pure elements. Indeed, fast-neutron reactions with a high-energy threshold are no longer possible, or at least they occur with a lower probability when the neutron energy spectrum is getting softer, especially deep inside hydrogenous cargo materials. Thus, as the pure elements database is no longer adapted, the unfolding algorithm may fail to identify the measured elements. To account for this bias, a systematic uncertainty is added to the conversion factors, in addition to the statistical one. During the identification procedure, it is accounted for by sampling the conversion factor over a uniform distribution for each of the hundred unfolding results.

The 2D likelihood histogram associated to the N/C and O/C fractions thus obtained is then represented in a barycentre triangle representation (see Fig. 9 (d)) inspired from the Dalitz plot in particle physics [16]. The N/C and O/C chemical ratio of common explosives, illicit drugs and benign materials are also projected in the triangle representation, which allows defining areas corresponding to these three types of materials. The overlap of the 2D likelihood map (corresponding to the current measurement) with these areas gives the probability that the measured organic compound is an explosive, an illicit drug or a benign material (see Fig. 9 (f)).

In order to facilitate understanding by non-expert end users, these results are summarized in a material distribution profile along the tagged beam direction, which is used to represent the evolution of the material type as a function of the depth in the container. In the example presented in Fig. 11, the container is filled with a metallic material (grey area), however, a red area, signing the presence of an explosive is clearly visible. The orange areas, corresponding to a chemical compound, visible over the whole length of the container correspond to artefacts due to statistical uncertainties in the unfolding procedure.

IV. Performance Tests

The performances of the RRTNIS and data processing have been tested at CEA Saclay using a container loaded with a 0.2 g.cm^{-3} iron or wood matrix in which a target of drug simulant, explosive simulant or benign material is hidden.
The wood matrix was constituted of sawdust bales, while the iron matrix was composed of variable sized iron boxes, filled with barbed wires.

Simulants were procured from both the Ruđer Bošković Institute (RBI) and the Dutch Customs Administration – Belastingdienst (DCA). Their compositions are given in Tables 1 and 2.

TABLE 1: COMPOSITION OF THE RDX AND TNT SIMULANTS PROCURED FROM RBI. DENSITY OF BOTH SIMULANTS IS 1.

Threat	Chemical formula	Chemical formula of simulant	Simulant Mass composition	O/C	N/C
Hexogen (RDX)	$C_3H_6N_6O_6$	$Si_3C_3H_6N_6O_6$	Melamine 0.412 Quartz sand 0.588	2	2
TNT	$C_7H_5N_3O_6$	$C_7H_6N_3O_6$	Graphite 0.158 Oxalic acid dehydrated 0.276 Cyanuric acid 0.566	0.86	0.43

TABLE 2: COMPOSITION OF THE COCAINE AND C4 SIMULANTS PROCURED FROM DCA.

Threat type	Chemical formula	Density	C	H	N	O	Cl	Si	S	O/C	N/C
Cocaine.HCl	$C_{17}H_{21}NO_4$	1.3	37.8%	48.9%	2.2%	8.9%	2.2%	-	-	0.23	0.06
C4	$C_8H_{16}N_{11}O_{11}$	1.0	16%	30%	21%	22%	-	11%	-	1.37	1.31

The measurements shown in Fig. 12 correspond to 10 min acquisitions with a neutron flux of $5 \cdot 10^7$ n/s. The material and CNO profiles allow identifying the material nature as well as its position in the matrix. In particular, explosive or narcotic simulants can be identified in the wood matrix through a change of the relative C, N and O proportions. More precisely, explosives are indicated by the presence of nitrogen, whereas drugs are detected because of an increase of carbon sufficient to shift the material type from benign to drug.

On the other hand, one can note that spurious explosive, chemical and drug are detected in the organic matrix, which is caused by the difficulty to unfold the gamma-ray spectra deeply in organic matrices. Indeed, a large contribution of scattered neutrons going at a lower speed than that of 14 MeV neutrons produce gamma rays at the beginning of the container [14]. These gamma rays have the same time of flight than gamma rays induced by non-scattered 14 MeV neutrons coming from the middle of the container overwhelm the gamma-ray spectrum. In addition, the pure element spectra that have been measured with 14 MeV neutrons are less relevant when going deeper in the container due to neutron slowing down. Given that gamma rays production cross section depends on the neutron energy, the slowed down neutrons affect the shape of the emitted gamma ray spectra. Finally, the statistics are poor due to neutron attenuation caused by the organic matrix.

These issues could be addressed by using a larger neutron flux, and/or a longer acquisition time. In addition, the unfolding database and algorithm could be modified to enable the use of pure element spectra associated to neutrons with an energy smaller than 14 MeV.

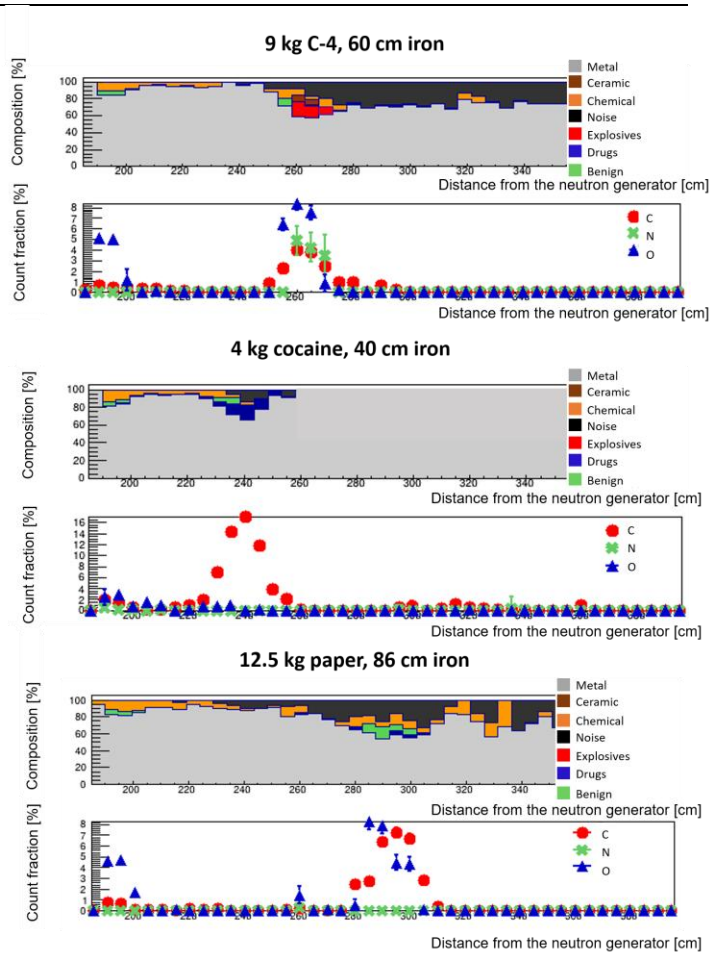

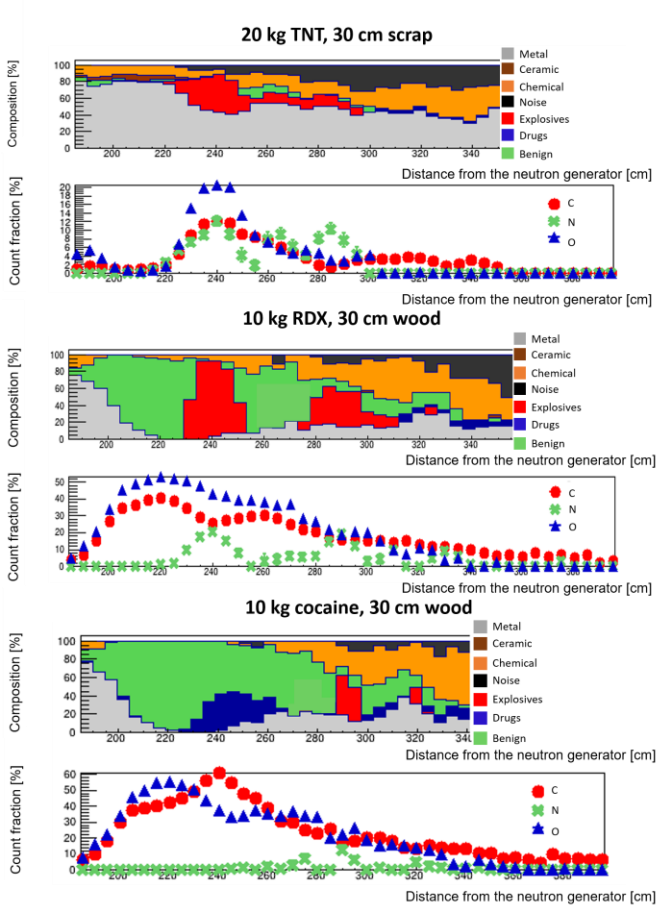

Fig. 12. Material and C, N, O count fraction profiles obtained during the 10 min measurement of different explosives, illicit drug simulants or paper targets placed inside iron or wood matrices. The red and blue spots sign the presence of explosives or narcotics, respectively. The material, its weight, the matrix nature and the thickness of matrix that the neutrons need to cross before reaching the target are indicated on top of each figure.

V. Conclusion

The Rapidly Relocatable Tagged Neutron Inspection System (RRTNIS) developed during the C-BORD project aims at providing a compact neutron interrogation system. The dedicated RRTNIS data acquisition electronics allows coincidences between the 20 NaI(Tl) scintillation detectors with the YAP detector that serves to tag the 14 MeV interrogating neutrons. The RRTNIS data processing allows labelling materials as organic, metallic, ceramic or chemical. Organic materials themselves are labelled as benign, explosives or illicit drugs depending on their carbon, oxygen and nitrogen chemical proportions deduced from their relative count contributions in the neutron-induced gamma ray spectra.

Experimental tests demonstrate that the system is able to identify less than 20 kg of explosives or narcotics in iron or wood matrices having a density of 0.2 $g.cm^{-3}$. Such performances constitute a real improvement compared to previous immovable EURITRACK Tagged Neutron Inspection System, designed to detect 100 kg of TNT in the middle of a 0.2 $g.cm^{-3}$ iron cargo [17], [18], [19].

Further improvements of the data processing are now foreseen in the frame of the new H2020 project ENTRANCE, which will start in October 2020, to improve material identification in the depth of the cargo container matrix, in particular with organic cargo materials. Artificial intelligence with fuzzy logic trees will be used to improve material classification. For example, recent studies showed that, although no hydrogen peak can be measured using tagged neutrons, the use of artificial neural networks allows assessing hydrogen concentration using the APT, thus improving greatly the capability to identify organic materials [20].

It is also worth noting the capability of tagged neutron inspection to detect other types of threats, like chemical [13], [21], and nuclear [12] [22] ones. The 20 large NaI detectors of the RRTNIS could also be used in passive mode to detect and identify radiological threats (dirty bomb) as any spectroscopic Radiation Portal Monitor [23]. The RRTNIS could therefore constitute an extremely versatile tool for the detection of CBRNE threats.

Acknowledgment

We would like to thank the following C-BORD Partners:

- Alessandro Iovene and Carlo Tintori of CAEN S.p.A. (Italy) for the development and commissioning of C-BORD's electronics.
- Bent Pedersen, Tatjana Bogucarska, Giovanni Varasano, Federica Simonelli, Hamid Tagziria and Franco Cioce of JRC Ispra (Italy) for welcoming the first RRTNIS integration tests.
- Łukasz Świderski and Krystian Grodzicki of NCBJ (Poland) for the realization and mounting of the RRTNIS polyethylene shield, as well as gamma detector supporting frame and lead shields.

References

[1] C-BORD Project - Effective Container Inspection at BORDer Control Points - Effective Container Inspection at BORDer Control Points." https://www.cbord-h2020.eu/ (accessed Nov. 19, 2020)

[2] P. Sibczynski *et al.*, "C-BORD - an overview of efficient toolbox for high-volume freight inspection," in *2017 IEEE Nuclear Science Symposium and Medical Imaging Conference (NSS/MIC)*, Atlanta, GA, Oct. 2017, pp. 1–3, doi: 10.1109/NSSMIC.2017.8532735..

[3] V. Valković, Đ. Miljanić, P. Tomaš, B. Antolković, and M. Furić, "Neutron-charged particle coincidence measurements from 14.4 MeV neutron induced reactions," *Nucl. Instrum. Methods*, vol. 76, no. 1, pp. 29–34, Dec. 1969, doi: 10.1016/0029-554X(69)90284-5.

[4] B. Perot *et al.*, "Development of the EURITRACK tagged neutron inspection system," *Nucl. Instrum. Methods Phys. Res. Sect. B Beam Interact. Mater. At.*, vol. 261, no. 1–2, pp. 295–298, Aug. 2007, doi: 10.1016/j.nimb.2007.03.073.

[5] A. Sardet *et al.*, "Design of the rapidly relocatable tagged neutron inspection system of the C-BORD project," in *2016 IEEE Nuclear Science Symposium, Medical Imaging Conference and Room-Temperature Semiconductor Detector Workshop (NSS/MIC/RTSD)*, Strasbourg, Oct. 2016, pp. 1–5, doi: 10.1109/NSSMIC.2016.8069693.

[6] D. A. Strellis, J. Stevenson, and T. Gozani, "Air cargo inspection using Pulsed Fast Neutron Analysis," International Atomic Energy Agency (IAEA), 2009. [Online]. Available: http://inis.iaea.org/search/search.aspx?orig_q=RN:40109362.

[7] C. L. Fontana *et al.*, "Detection System of the First Rapidly Relocatable Tagged Neutron Inspection System (RRTNIS), Developed in the Framework of the European H2020 C-BORD Project," *Phys. Procedia*, vol. 90, pp. 279–284, 2017, doi: 10.1016/j.phpro.2017.09.010.

[8] F. Pino *et al.*, "Advances on the development of the detection system of C-BORD's rapidly relocatable tagged neutron inspection," *Int. J. Mod. Phys. Conf. Ser.*, vol. 48, p. 1860125, Jan. 2018, doi: 10.1142/S2010194518601254.

[9] A. Sardet *et al.*, "Gamma signatures of the C-BORD Tagged Neutron Inspection System," *EPJ Web Conf.*, vol. 170, p. 07011, 2018, doi: 10.1051/epjconf/201817007011.

[10] M. Gierlik *et al.*, "Comparative study of large NaI(Tl) and BGO scintillators for the EURopean Illicit TRAfficking countermeasures kit project," *IEEE Trans. Nucl. Sci.*, vol. 53, no. 3, pp. 1737–1743, 2006, doi: 10.1109/TNS.2006.875150.

[11] V. Valkovic *et al.*, "The use of alpha particle tagged neutrons for the inspection of objects on the sea floor for the presence of explosives," *Nucl. Instrum. Methods Phys. Res. Sect. Accel. Spectrometers Detect. Assoc. Equip.*, vol. 703, 2013, doi: 10.1016/j.nima.2012.11.096

[12] B. Perot *et al.*, "Detection of special nuclear materials with tagged neutrons," in *2016 IEEE Nuclear Science Symposium, Medical Imaging Conference and Room-Temperature Semiconductor Detector Workshop (NSS/MIC/RTSD)*, Strasbourg, Oct. 2016, pp. 1–4, doi: 10.1109/NSSMIC.2016.8069917.

[13] B. Perot *et al.*, "Materials characterisation with the Associated Particle Technique," 2012, pp. 1702–1711, doi: 10.1109/NSSMIC.2012.6551402.

[14] C. Carasco *et al.*, "Photon attenuation and neutron moderation correction factors for the inspection of cargo containers with tagged neutrons," *Nucl. Instrum. Methods Phys. Res. Sect. Accel. Spectrometers Detect. Assoc. Equip.*, vol. 582, no. 2, pp. 638–643, Nov. 2007, doi: 10.1016/j.nima.2007.09.002

[15] W. El Kanawati *et al.*, "Conversion factors from counts to chemical ratios for the EURITRACK tagged neutron inspection system," *Nucl. Instrum. Methods Phys. Res. Sect. Accel. Spectrometers Detect. Assoc. Equip.*, vol. 654, no. 1, pp. 621–629, 2011, doi: 10.1016/j.nima.2011.05.076.

[16] R. H. Dalitz, "Decay of τ Mesons of Known Charge," *Phys. Rev.*, vol. 94, no. 4, pp. 1046–1051, May 1954, doi: 10.1103/PhysRev.94.1046.

[17] G. Perret, B. Perot, J.-L. Artaud, and A. Mariani, "EURITRACK tagged neutron inspection system design," *J. Phys. Conf. Ser.*, vol. 41, pp. 375–383, May 2006, doi: 10.1088/1742-6596/41/1/041.

[18] A. Donzella *et al.*, "Experimental validation of MCNP simulations for the EURITRACK Tagged Neutron Inspection System," *Nucl. Instrum. Methods Phys. Res. Sect. B Beam Interact. Mater. At.*, vol. 261, no. 1-2 SPEC. ISS., pp. 291–294, 2007, doi: 10.1016/j.nimb.2007.03.090.

[19] C. Carasco *et al.*, "In-field tests of the EURITRACK tagged neutron inspection system," *Nucl. Instrum. Methods Phys. Res. Sect. Accel. Spectrometers Detect. Assoc. Equip.*, vol. 588, no. 3, pp. 397–405, Apr. 2008, doi: 10.1016/j.nima.2008.01.097

[20] C. Carasco, B. Pérot, and A. Sardet, "Measuring hydrogen with fast neutrons: Application to organic materials identification in cargo containers," *Nucl. Instrum. Methods Phys. Res. Sect. Accel. Spectrometers Detect. Assoc. Equip.*, vol. 951, p. 163030, Jan. 2020, doi: 10.1016/j.nima.2019.163030.

[21] B. Perot *et al.*, "Acquisition of neutron-induced gamma signatures of chemical agents," presented at the International Topical Meeting on Nuclear Research Applications and Utilization of Accelerators, 2009, [Online]. Available: https://www.scopus.com/inward/record.url?eid=2-s2.0-79952777316&partnerID=40&md5=83581433c354ead4d67273a56c0f121c

[22] C. Deyglun *et al.*, "Passive and active correlation techniques for the detection of nuclear materials," *IEEE Trans. Nucl. Sci.*, vol. 61, no. 4, pp. 2228–2234, 2014, doi: 10.1109/TNS.2014.2315714.

[23] R. C. Runkle, M. F. Tardiff, K. K. Anderson, D. K. Carlson, and L. E. Smith, "Analysis of spectroscopic radiation portal monitor data using principal components analysis," *IEEE Trans. Nucl. Sci.*, vol. 53, no. 3, p. 6, 2006